FULL PAPER

Multiscale Pattern Generation in Viscoelastic Polymer Films by Spatiotemporal Modulation of Electric Field and Control of Rheology

Partho S. G. Pattader, Indrani Banerjee, Ashutosh Sharma, and Dipankar Bandyopadhyay*

Electric-field-induced hierarchical, multiscale patterning of incompletely cross-linked viscoelastic polydimethylsiloxane (PDMS) films is achieved by spatiotemporal variation of the field, which produces a multiplicity of complex mesopatterns from the same electrode. Experiments and simulations are employed to uncover pathways of hierarchical pattern formation. Spatial modulation of the field is introduced by employing different types of simply patterned electrodes: stripes, elevated concentric circular rings, and box-patterned ridges. Multiscale complex structures consisting of increasingly finer primary, secondary, and tertiary hierarchical structures are fabricated by progressively ramping up the electric field while maintaining the integrity of the already formed structures. The latter is achieved by partially cross-linking the films before patterning, which engenders optimal viscosity to prevent a rapid ripening and coalescence of earlier formed patterns. These multiscale structures can be controlled by the geometry and periodicity of patterned electrodes, the strength of the electric field, and its programmable temporal variation. The PDMS patterns are made permanent by complete cross-linking after a desired multiscale structure is obtained.

1. Introduction

Pattern formation in thin polymer films by exploiting the instabilities engendered by the intermolecular forces,[1–29] residual stresses,[30–32] contact forces,[33–42] lithographically induced self assembly (LISA),[43–45] and externally applied electric field[46–82] has been extensively studied. Rapid miniaturization of the technological devices has made these patterns useful in a variety of mesoscale product or processes such as coatings, micro-adhesives, microelectronics, micro/nanofluidic devices, and superhydrophobic surfaces. Thin polymer films also serve as simple prototypes for the fundamental studies on dewetting, adhesion, debonding, adsorption, and phase transition.

Thin soft polymer films become unstable when subjected to an external electric field and can readily self-organize into micro/nano architectures such as columns, channels, cavities and holes under different conditions.[47–82] It is now well understood that liquid (solid) interfaces show instability in the form of these patterns when the destabilizing electric field overcomes the stabilizing surface tension force (elastic strain energy). The wavelength of the electric field induced patterns depends on the applied field which in turn depends on the film thickness, applied voltage and the gap distance between the two electrodes.[47,48,52,56,65,66] Large-area ordering becomes possible for columnar, doubly periodic,[53] and phase inverted[63] microstructures by imposing a spatial variation in the field[65,66,68,73,77,78,80] via patterned electrodes. Electric field lithography (EFL) using a spatially varying field is thus emerging to be an effective method for generating ordered meso structures in soft polymers, both in liquid and solid viscoelastic films.

In this study, we propose the use of a spatiotemporally varying electric field and tailoring of the PDMS rheology to fabricate large area hierarchical, mesopatterns directly in PDMS, which is the most popular soft-lithography material for generation of molds, stamps and master patterns. We show that a temporally varying field offers the possibility of producing multiscale patterns and multiple patterns from the same electrode. With the help of experiments and simulations, we show some of the key features of fabrication of hierarchical structures in PDMS by the proposed Temporally Modulated-Electric Field Lithography Tool (TeMo-EFL).

The electric field induced patterns in polymer films can be generated following two different methodologies: a) by heating the polymer above its glass transition temperature (T_g) or by

P. S. G. Pattader, I. Banerjee, Prof. A. Sharma
Department of Chemical Engineering
Indian Institute of Technology
Kanpur 208016, UP, India
Tel: +91–512-259 7026
Fax: +91–512-259 0104
E-mail: ashutos@iitk.ac.in
Prof. A. Sharma
School of Mechanical Engineering
Yeungnam University
Gyongsan 712–749, South Korea
Dr. D. Bandyopadhyay
Department of Chemical Engineering
Indian Institute of Technology
Guwahati 781039, Assam, India

DOI: 10.1002/adfm.201001206

reducing its T_g by a solvent vapor followed by patterning and then reducing the temperature below T_g to freeze the structures,[47] or b) by patterning soft photo/UV curable liquid polymers followed by their rapid curing before removal of the top electrode.[70] Laser heating for self-organization in thin metallic films is another possibility, not yet explored for polymer films.[19] Patterned cross-linkable polymers such as PDMS are of course the mainstay of a variety of soft lithography techniques requiring moulds, stamps, templates and masters. We propose and demonstrate here a new variant of electric field lithography (TeMo-EFL) for multiscale patterning of PDMS by its initial partial cross-linking to increase its viscosity significantly, then employing spatiotemporal variations of the electric field and subsequent complete thermal-curing before removing the top-electrode.

Multiscale patterns of increased complexity are not easily fabricated by EFL unless the electrode template has the same structure imprinted on it, nor is a multiscale template structure faithfully replicated in the film under a given set of conditions because of the e-field instability length-scale not being commensurate simultaneously with all the different scales on the template. The length-scale of the pattern formed decreases with increase in the field intensity.[47,48,52,56,65,66] We thus use a simple patterned electrode with a single periodicity, but employ temporal variation of the electric field to fabricate multiscale hierarchical structures by changing the instability length-scale with time. A key challenge in this strategy is to preserve the integrity of the already formed structures as newer finer structures are formed by intensifying the field and also to minimize the change in the liquid structures while postcuring to make them permanent. We show that the viscosity of commonly used non-crosslinked PDMS (e.g., Sylgard) is not appropriate for this task and does not offer enough flexibility as regards the formation of multiscale structures by the temporal variation of the field. This is because the structures already formed ripen, distort and/or coalesce readily unless made permanent by complete cross-linking, in which case the subsequent finer structures cannot be formed. This problem could be circumvented by a partial cross-linking of PDMS which still retains its viscoelastic liquid nature, but with greatly increased viscosity that significantly slows down the dynamics of ripening/coarsening of structures so that the structural integrity is maintained even while the new structures are being formed. A spatially varying *field* as a tool of parallel mesofabrication is already an interesting and intriguing approach compared to the use of a *physical* microtool, which is usually a serial process. The approach proposed here makes the tool-kit of field patterning complete by adding the temporal dimension to the spatial field variation. This allows far greater flexibility in fabrication of complex multiscale structures. For example, a variety of different structures can be fabricated using the same simple electrode-template, but by changing the temporal variation of the field which is an easily controllable variable.

In what follows, we show both experiments and simulations to investigate the effects of field strength and its spatiotemporal variation on the formation of hierarchical mesostructures. In the experiments, a commercially available Sylgard 184 was used, which contains a base polymer and a cross-linker. The overall experimental procedure can be divided into five steps: I) a cross-linker mixed PDMS film is spin-coated on a conducting substrate; II) the film is precured partially by heating for a short duration to induce greater viscosity and viscoelastic properties, by which a desirable rheology could be optimized; III) in the patterning phase, the electric field induced patterns are fabricated in the PDMS film by employing a simply patterned top electrode and by changing the applied voltage with time; IV) in the postcuring phase, the patterned film is completely cross-linked or cured by a more intense heat treatment; V) Finally, the top electrode is removed after complete curing.

2. Results and Discussion

2.1. Optimization of the Precuring Time

Application of electric field generates stress on the surface of a polymer film and columnar structures are thus formed. **Figure 1** schematically shows the experimental setup [images (a) to (d)] and theoretical [image (e)] sketch employed in this study for thin films deforming under flat [images (a) and (b)] and patterned electrodes [images (c) to (e)]. The length scale (λ) of instability in a flat film deforming under electric field clearly suggests that the mean spacing between the columns formed largely depends on the applied voltage (ψ), the film thickness (h) and the distance between the two electrodes (d).[47,48,52,56,65,66] The dependence of λ on ψ, h and d can be found in the Equation (4)

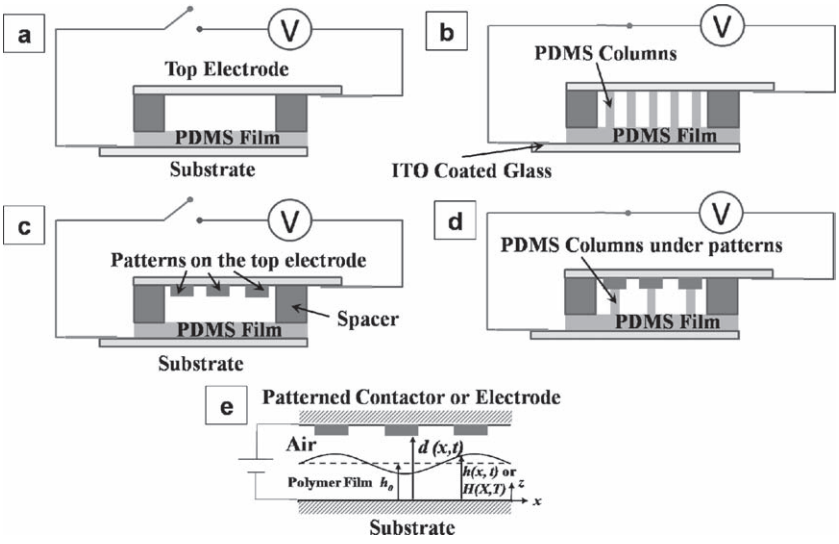

Figure 1. Schematic diagrams of a polymer film resting on a rigid substrate and under the influence of an electric field. The images (a) and (b) show the experimental setup of an initially flat thin film deforming into columns under a uniform electric field. The images (c) and (d) show the experimental prototype of thin film deformation under a patterned electrode. Image (e) shows simulated setup of a thin film deforming under a spatially varying electric field.

of theory and simulation section. At a later stage of evolution, the columns coalesce because of the gradient in the Laplace pressure ensuing from the difference in the size of the columns across the space. Interestingly, this late stage ripening of structures continues even when the electric field is turned off. Thus, in addition to finding the conditions required to obtain a particular ordered structure, it is also important to understand the pathways of coarsening in order to preserve the structures already formed. Partial precuring transforms the cross-linker filled low viscosity liquid PDMS films to highly viscous films. When these films are patterned, the increased viscosity helps in retaining the fabricated patterns by slowing down the processes of flow, pattern transformation and ripening.

Figure 2 shows the influence of precuring time on the late stage coalescence of the patterned structures. Figure 2a and 2c show the short time morphologies on application of electric field, when the films are precured at 105 °C for ~10 min and ~30 min, respectively. Figure 2b and 2d show that the ripening/coalescence of the patterned structures are high at the later stages, which leads to loss of order in the postcuring phase. In contrast, Figure 2e and 2f show that when the films are precured at 105 °C for ~45 min, the late stage ripening can be reduced considerably and ordering of columns can be preserved even after removal of the top electrode (Figure 2f). These experiments also reveal that the films precured at 105 °C for more than 60 min leads to nearly elastic PDMS films, which do not yield even under exposure to a moderately strong electric field. The rheology of films cured for more than 60 min were similar to the films that are completely cured at cross-linker concentrations of 2% or more,[81] corresponding to a solid viscoelastic regime with G' (elastic modulus)>> G'' (loss modulus). Thus, we employed the optimum range of 45 to 60 min of precuring before applying the electric field to fabricate patterns which retain their morphology during the patterning and postcuring phase. The viscoelastic rheology of these films was similar to the films that are completely cured at much lower cross-linker concentrations of around 1%[81] corresponding to a liquid viscoelastic regime.

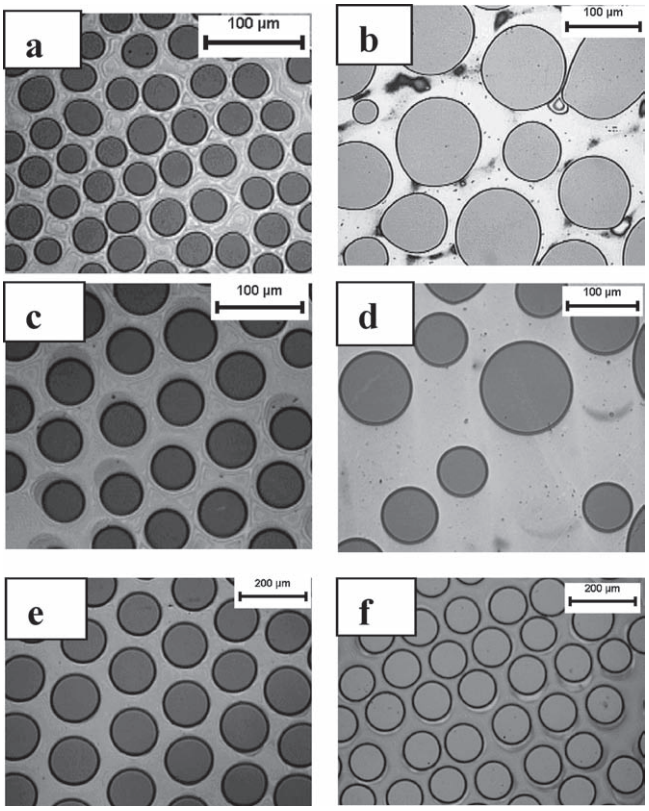

Figure 2. Optical micrographs of PDMS surfaces under the influence of a 30 V electric field bias. The films are precured at 105 °C for: a) 10, c) 30, and e) 45 min. The film thicknesses are: a) 6.4, c) 5.0, and e) 10 µm. Images (b), (d) and (f) are the optical micrographs corresponding to (a), (c) and (e) after 24 h of postcuring. The darker shades in the images represent the regions in contact with the top electrode. Image (f) shows the patterns after removal of the top electrode.

2.2. Alignment of Patterns Employing Patterned Electrodes

Patterned electrodes impose a spatial variation in the gap distance between the surface of the polymer film and the top electrode. In consequence, the higher field strength shifts the preferred zone of column formation to the places where the top electrode is closest to the film surface. Synchronization between the pattern periodicity on the top electrode and the natural wavelength (λ) of the electric field induced instability helps in the ordering of the columns formed. In this section, we show the conditions to generate ordered patterns in PDMS using a patterned top electrode and preservation of these patterns.

Figure 3 shows the sketches of the patterned electrodes used in this study: a) alternate parallel ridges and grooves, b) elevated concentric circular rings, and c) elevated isolated boxes. The patterned electrodes were fabricated using photolithography and positive photo-resist, Shipley 1818. The elevated portions on the top electrode are termed as 'ridges', which is closer to the film surface. The grooves on the top electrode that are away from the film surface are termed as 'valleys'.

Figure 4 shows the ordered structures formed using an electrode with alternate stripes of ridges and valleys (Figure 4a). The portions containing the ridges (darker region in Figure 4a) are nearer to the film surface by a distance equal to the height

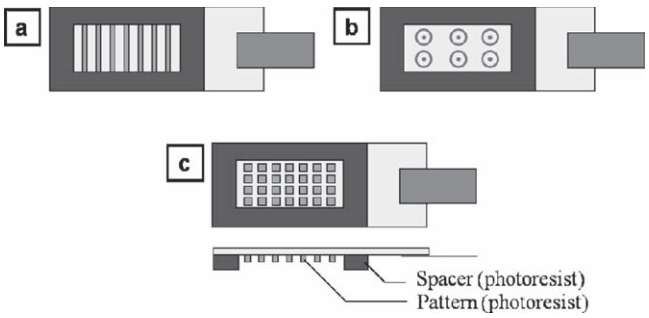

Figure 3. Sketches of the different types of patterned top electrodes employed. Image (a) shows alternate parallel ridges (darker shades) and valleys (lighter shades), image (b) shows elevated concentric circular rings (darker shades) and image (c) shows elevated isolated boxes (darker shades). In all images the spacer photo-resist is marked by the darker rectangular shade surrounding the patterns.

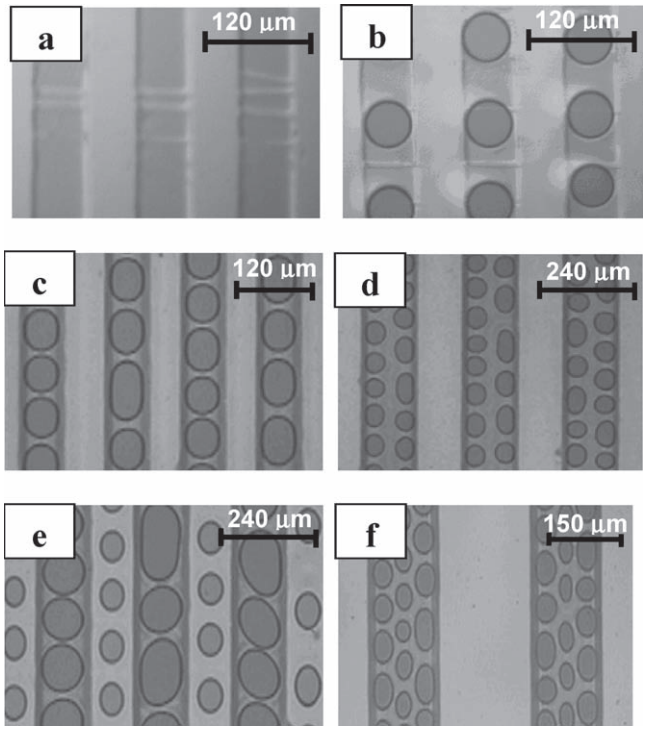

Figure 4. Image (a) shows a topographically patterned electrode fabricated with alternate parallel ridges (darker gray shades) and grooves (lighter gray shades). Darker regions are closer to the polymer film surface. Image (b) shows formation of columns on the ridges when 30 V bias is applied on a polymer film of $h = 9$ µm. The pattern periodicity at the patterned electrode is L_P (120 µm) is nearly equal to λ (~105 µm). Image (c) shows ordered columns on the ridges when 38 V voltage bias is applied on a polymer film of thickness $h = 6.7$ µm. In this case, the width of ridges, $w = 60$ µm (~$\lambda = 55$ µm) and $L_P = 120$ µm (>λ). Image (d) shows an array of doublet of columns per stripe when the same experiment is carried out as in image (c), but the stripe width is increased to w = 120 µm (~2λ). Image (e) shows the interfacial morphologies when the image (d) structures are further exposed to a voltage bias of 70 V for 8 min duration. The columns on the ridges coalesce and new array of columns appear at the grooves. Image (f) shows an array of triplet of columns per stripe is when the same experiment is carried out as in image (a) and (c) but the stripe width is increased to w = 150 µm (~3λ).

of the ridges. Figure 4b shows that application of electric field leads to the formation of columns under the ridges of the top electrode. Experiments suggest that a row of single columns on the ridge can be fabricated not only when the periodicity of the stripes (L_p) approximately matches the theoretically obtained wavelength, λ, of electric field induced instability, but the row persists even when $L_p > \lambda$. In fact, the number of arrays of columns formed per stripe is governed by the stripe width (w) of the patterned electrode vis-à-vis λ. Figure 4c shows an example where L_p is much larger than λ, but a row of single columns are still formed per stripe because in this case $w \sim \lambda$. However, a comparison between the Figure 4b and 4c reveals that the columns lose their circular shape when $L_p > \lambda$. Further, Figure 4d (Figure 4f) shows that when $w \sim 2\lambda$ (3λ), a double (triple) array of columns are formed per stripe. The linear order imposed by the electrode pattern is still followed by the PDMS columnar arrays. Figure 4 also shows that the mean spacing between the columns in the transverse direction is dictated by the natural wavelength λ. It is also interesting to note here that after fabricating the ordered structures in Figure 4d at 38 V, if the voltage is subsequently ramped up to 70 V, a newly formed row of columns at the valleys of the patterned contactor is observed (Figure 4e). These columns are smaller in diameter because they are formed at higher voltages. In addition, they are taller than the columns below the ridges of the patterned electrode because of the larger gap distance between the film surface and the valleys on the top electrode. Furthermore, Figure 4e shows that if the electric field exposure of 70 V is continued for ~8 more min, the columns under the ridges of the top electrode coalesce and form a row of single columns per stripe.

In contrast to the one dimensional stripes as shown above, fabricating the top electrode with a more complex shape, for example, elevated concentric circular rings leads to two-dimensional ordering. **Figure 5** shows patterned PDMS films by employing a top electrode with concentric rings. The radius of the inner ring (R_1) and the outer ring (R_2) quantifies the lateral spacing of the patterns fabricated on the top electrode (Figure 5a). Application of electric field in such systems leads to the formation of columns along the circular ridges of the top electrode as shown in Figure 5b. A single array of ordered columns is formed even when the pattern periodicity is greater than λ but the width of each circular ring is less than 2λ (Figure 5b). Experiments also show that after some time these columns coalesce to form a continuous positive replica of the top electrode (Figure 5c). At a later stage of evolution, progressive appearance of pillars is also observed in the valleys of the top

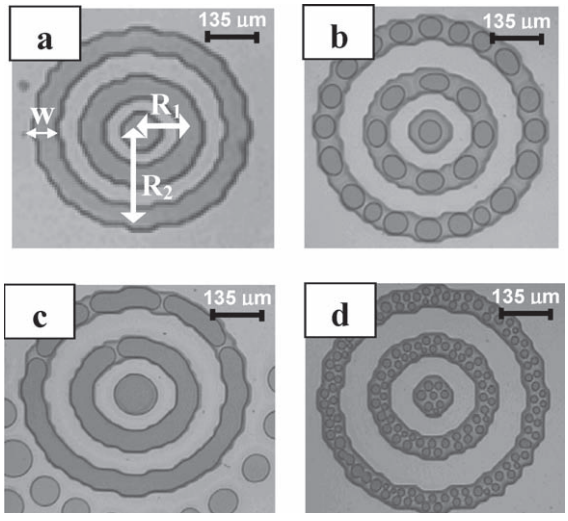

Figure 5. Image (a) is the elevated concentric circular ring electrode with $R_1 = 135$ µm, $R_2 = 2R_1$ and $w = 60$ µm. The darker shades of gray on the patterned contactor are closer to the surface of the polymer film. Images (b)–(c) show the structure formation in 8 µm thick film. Image (b) shows the appearance of single row of columns along the circular ring of the electrode within 30 s of electric field exposure (25 V) when w < λ (=106 µm). Image (c) shows the coalescence of the columns under the circular ring when applied voltage bias of 25 V is maintained for 10 min. Image (d) shows the appearance of doublet of columns when film thickness $h = 3.84$ µm and voltage bias is 30 V. In this case, each circular ring of the electrode has a width, w (60 µm) roughly equal to 2λ ($\lambda = 31$ µm).

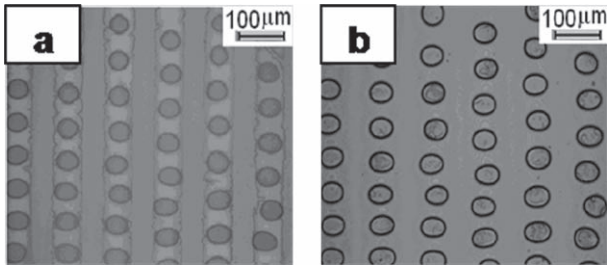

Figure 6. Ordered patterning on a patterned electrode with parallel grooves and ridges with a voltage bias of 30 V on a film of thickness 6.5 μm. The wavelength calculated theoretically, $\lambda = 68$ μm is close to the width of each stripe $w = 55$ μm. Image (a) shows the structures formed after application of the electric field and Image (b) shows the structures after curing the film at 120 °C for 24 h followed by removal of the top electrode.

electrode (Figure 5c). Figure 5d shows that if the width of the circular ring is greater than 2λ then a circular array of doublet of columns appears under each circular ring, which also undergoes coalescence at later time (not shown). The above findings emphasize the importance of time even under a constant voltage in producing very distinct structures. Freezing these structures in PDMS at different times at different stages of evolution thus allows a more flexible approach to patterning. **Figure 6** shows one such example where an ordered one-dimensional array of columns is generated under the ridges of a patterned electrode (Figure 6a) and then postcured for 24 h at 120 °C without the removal of the top electrode. Figure 6b shows the array of columns thus made permanent without the loss of their original definition even after the removal of the top electrode. These permanent patterns in PDMS can be further employed as stamps or moulds in various microfabrication techniques and soft lithographies.

2.3. Hierarchical Patterning by Temporal Variation of Electric Field

It is already known that the radius and spacing of the columns depend on the strength of the electric field.[47,48,52,56,65,66] In this study, we employ this particular aspect of electric field induced instability of polymer films to fabricate multiscale hierarchical structures. For example, **Figure 7** shows an experiment where a 5 μm film under a flat top electrode generates hexagonally packed primary columns of ~ 100 μm diameter when a 30 V electric field is applied. After fabricating these large columns, the electric field strength was ramped up to 70 V, which resulted in an array of secondary columns of much smaller size in the interstitial spaces surrounding the primary columns. The experiment demonstrates that secondary structures can be fabricated by varying the electric field strength in time before any significant change occurs in the primary structure.

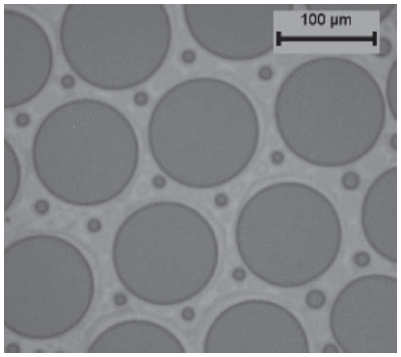

Figure 7. Columns with larger diameter formed when a 5.0 μm thick film is exposed to a 30 V electric field bias. The columns with smaller diameter at the interstitial spaces appear when the voltage bias is ramped up to 70 V. The darker regions in the figure represent the regions in contact with the top electrode.

The order and complexity of hierarchical patterns thus obtained can be vastly increased by employing patterned electrodes. **Figure 8** shows an example of hierarchical patterning employing a patterned top electrode with alternate stripes of ridges and valleys ($w = 120$ μm). Images (a)–(c) depict the experimental results and the images (i)–(iv) show the results obtained from the numerical simulations, the methodology of which is discussed in the theory section at the end. The same methodology for simulations has been found to give excellent agreement with the experiments on electric field patterning by topographically patterned electrodes, including the stages of column formation and their late time transformations and coarsening.[64,65,68,77] Image (a) shows that when the PDMS film is subjected to an electric field bias of 40 V, a double array of columns is observed under the ridges of the top electrode, as expected. The stripe width ($w = 120$ μm), voltage bias, film thickness and the gap between the electrodes indicate that the lateral separation distance of the columns follow the natural length-scale of electric field induced instability. At this stage, the voltage bias was increased to 65 V, resulting in arrays of single secondary columns that formed under the valleys of the top electrode, as depicted in Image (b). Thereafter, the voltage bias was further ramped up to 130 V, which allowed the formation of tertiary columns with much smaller diameter at both sides of the columns fabricated under the valleys as in Figure 8c. It is interesting to note here that the tertiary columns are formed in the transverse direction also in between two successive secondary columns. Also, the locations of the secondary columns are out-of-phase with the primary columns. The experiment shown in Figure 8 is also simulated to identify the details of the pathways of these evolutions. Image (i) in Figure 8 shows the patterned top electrode used for the simulation with stripe width of 2.85λ at the initial voltage applied. When the voltage bias is kept to 40 V, a double array of columns appears under the ridges as shown in image (ii). Thereafter, the ramping up of the voltage to 70 V leads to coarsening and then coalescence of structures under the ridges and formation of secondary columns under the grooves [image (iii)]. Finally, when the voltage is increased to 130 V, tertiary columns appear on both sides of the secondary columns [image (iv)]. It is interesting to note here that although the various stages in simulated patterns closely mimic the experimental ones, the rate of coalescence is found to be much faster in the simulations. This can be attributed to the fact that the films in the simulations are considered to be purely viscous, whereas the films used for the experiments are weakly viscoelastic.

The above experiments together with the simulations highlight the following important points: i) ordered arrays of

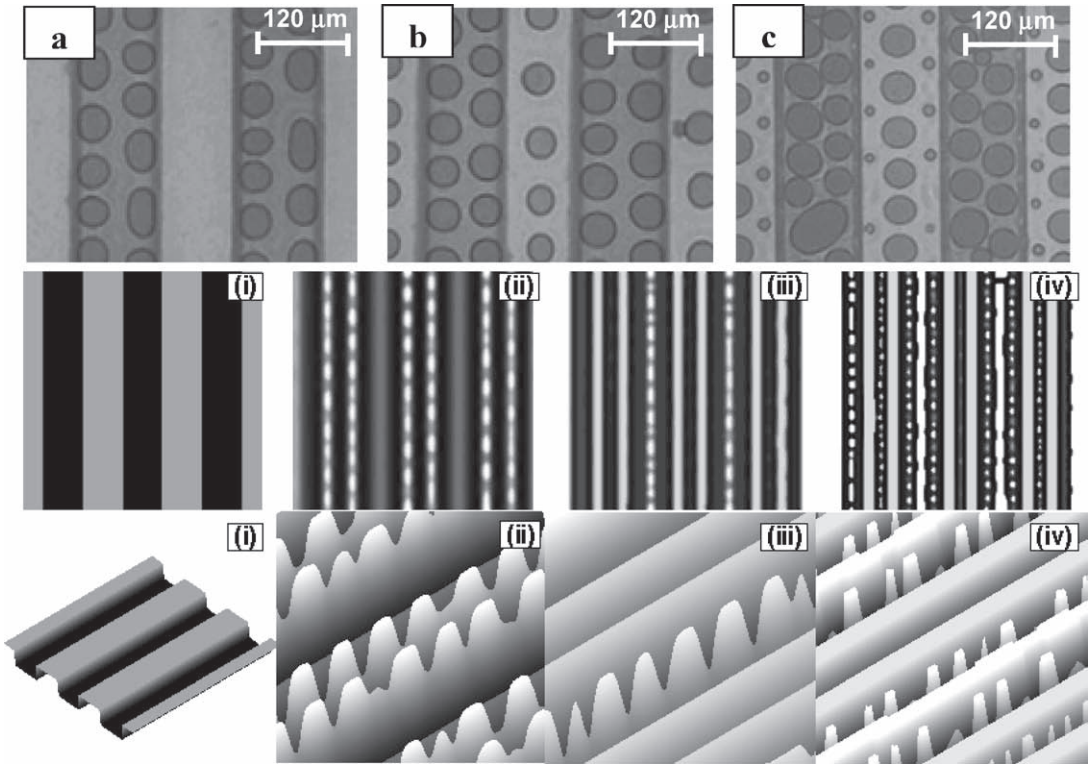

Figure 8. Optical micrographs (a)–(c) show patterning of a 7 μm film under a top electrode having parallel ridges and stripes of $w = 120$ μm. Image (a) shows an array of doublet-columns when electric field bias is 40 V ($w \sim 2\lambda$). Image (b) shows appearance of columns under grooves of the top electrode when the electric field bias is ramped up to 65 V for 2 min. Image (c) shows the emergence of ordered thinner columns at the grooves of the patterned electrode when the voltage bias is further increased to 130 V. Images (i)–(v) show the simulated patterns on a 7 μm film under a patterned electrode having the stripe width of 2.85λ. The dimensionless distance of the ridges [black stripes in Image (i)] and grooves [gray stripes in Image (i)] of the patterned electrode from the film surface are 2.0 and 2.1, respectively. Image (ii) shows an array doublet-columns per stripe under the ridges of the patterned electrode at 40 V and $T = 2.07 \times 10^3$. Image (iii) is appearance of secondary columns under the grooves of the top electrode when the voltage is ramped up to 70 V and $T = 2.37 \times 10^3$. Image (iv) is emergence of smaller tertiary columns at the grooves when the voltage is further ramped up to 130 V and $T = 2.67 \times 10^3$. In the simulated pictures the lighter shades of gray indicate the regions with higher film thickness.

columns of differing heights and diameters can be generated by changing the field strength, bias duration and the patterns on the top electrode; ii) changing the precise temporal variation of electric field changes the pattern. For example, two experiments shown in Figure 8a and Figure 4d both started with the formation of a double array of columns. However, ramping up the voltage to 70 V and exposing film to the electric field bias for 8 min led to the coalescence of columns and finally a single array of columns per stripe resulted along with the appearance of secondary columns under the grooves, as shown in Figure 4e. In contrast, if the voltage was increased immediately to 130 V after the formation of the columns under the valleys of the top electrode (at the stage shown in Figure 8b) a completely different microstructure appeared as shown in Figure 8c. iii) It may be noted that in the initial stages after ramping up the voltage, the column diameters increase by the process of ripening where first material flows into columns from the films at their bases and later flow occurs from the smaller to the larger columns. True coalescence can occurs once the excess material in the film is depleted and the columns grow large enough to be in closer vicinity. Thus, the initial coarsening dynamics where the microstructures grow in width/diameter under a stronger electric field can be differentiated from coalescence where smaller structures are merged into the larger ones. The simulations and experiments shown in Figure 8 and the subsequent figure demonstrate the coexistence of the coarsening and coalescence phenomena at the late stages.

The importance of the strength of electric field and its temporal variation in determining the structure are shown more explicitly in the **Figure 9**, **10**, and **11**. These figure illustrate that by employing the same electrode, but by altering the field strength and its temporal variation, a variety of distinct ordered hierarchical structures can be fabricated.

Image (a) of Figure 9 shows the optical micrograph of the top electrode used in these experiments. The electrode contains an array of square boxes (150 μm x 150 μm) projecting (~1 μm) towards the film surface and isolated by 30 μm channels. Image (b) shows application of 20 V electric field bias on a 7.7 μm PDMS film produces a single column at the center of each box. The applied voltage, film thickness and the gap distance between the electrodes ensure that the size of each box is much less than 2λ. After 1 min, the applied voltage is increased to 50 V, which now causes the formation of

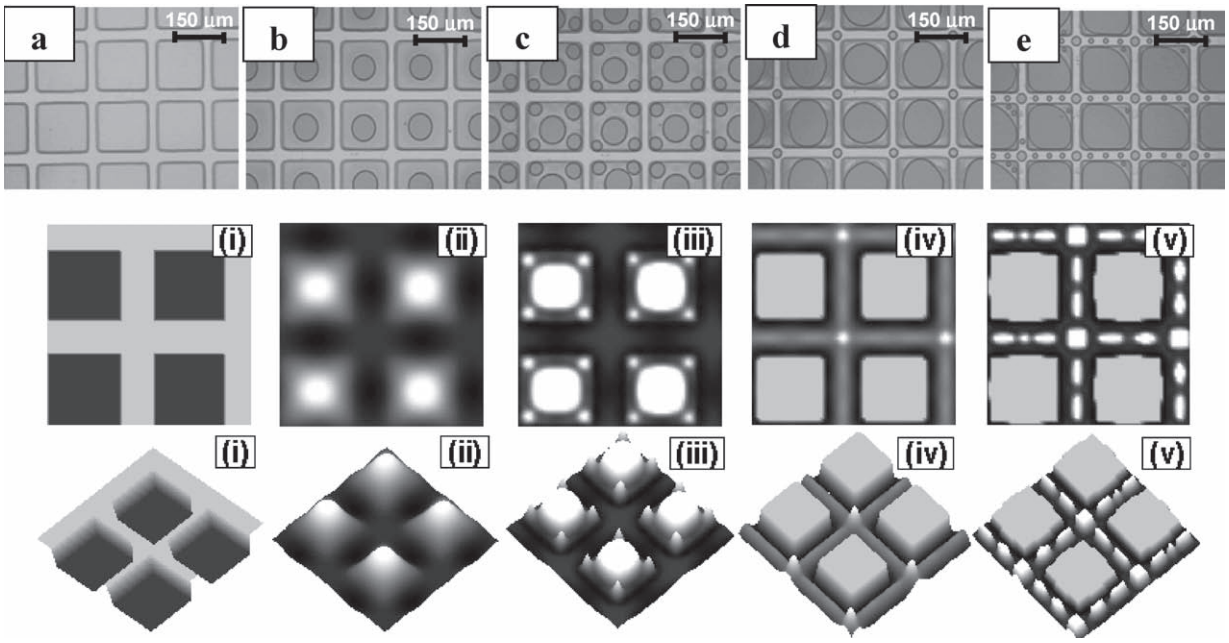

Figure 9. Optical micrographs (a)–(e) show patterning of a 7.7 μm film. Image (a) shows a box-patterned top electrode with elevated square boxes of dimension 150 × 150 μm. The height of the boxes are ~1 μm. Image (b) shows formation of one primary column per box under the voltage bias of 20 V after 1 min (box dimension ~ λ). The voltage is then ramped up to 50 V for 1 min and the image (c) shows the appearance of four secondary columns per box. Thereafter, voltage is again ramped up to 100 V for 4 min and image (d) shows the appearance of tertiary columns under the grooves and at the corners of the box-patterns. When the voltage is again increased to 130 V for another 4 min, image (e) shows the formation of quaternary columns in the channels between the boxes. Images (i)–(v) show simulated patterns on a 7 μm film under a patterned electrode having boxes of dimension 1.06λ. The dimensionless distance of the boxes [darker region in image (i)] and grooves [lighter region in image (i)] on the patterned electrode from the film surface are 1.6 and 2.0, respectively. Image (ii) shows single primary column per box at 20 V and $T = 9.4 \times 10^2$. Image (iii) shows the appearance of secondary columns at the corner of the boxes at 65 V and $T = 9.5 \times 10^2$. Image (iv) shows coalescence of structures under the boxes and appearance of tertiary columns under the grooves at the corner of the box-patterns when the voltage is ramped up to 100 V at $T = 1.01 \times 10^3$. Image (v) shows appearance of quaternary columns under the grooves and in between the box patterns when the voltage bias is ramped up to 130 V at $T = 1.04 \times 10^3$. In the simulated pictures, lighter shades of gray indicate the regions with higher film thickness.

secondary columns with smaller diameter at the four corners of each box as shown in image (c). The total number of columns in each box thus increases to five at this stage of evolution. After exposing the film to 50 V for 1 min, the applied voltage is further ramped up to 100V in image (d). In response, the five columns already formed on each box initially coarsen and then coalesce to form a single large column under each box and smaller tertiary columns start to appear at the intersection of the channels surrounding the boxes (in the grooves of the top electrode) [image (d)]. After 4 min of exposure to 100 V bias, the voltage is further ramped up to 130V in image (e), causing the appearance of small, equal-spaced quaternary columns all along the length of channels as shown in image (e). Simulated images (i)–(v) show the morphological evolution for these conditions, which mimics the various stages of experimental results. Image (i) shows the box-patterned top electrode with box dimension 1.06λ with respect to the initial voltage applied. In the beginning a 20 V electric field is applied to the film and one column at the center of each box can be seen [image (ii)]. Further, when the voltage is ramped up to 65 V, four secondary columns do indeed appear at the corners of each box [image (iii)]. Thereafter, increasing the voltage to 100 V leads to the coarsening and coalescence of all the pillars and analogous to the experiments, tertiary columns start appearing under the grooves and at the corners of the boxes as shown in the image (iv). Finally, when the electric field is further stepped up to 130 V, quaternary columns are observed in the channels.

In Figure 10, we show that using the same top electrode and a PDMS film of thickness 7.7 μm, a new set of morphologies can be decorated by tuning the applied voltage and its history. On application of an initial 30 V, a quartet of primary columns directly appears on each box as shown in image (a). In this case, the applied voltage, gap distance between the electrodes and the film thickness chosen ensure that the width of the box is greater than 2λ. After 30 s, the voltage is ramped up to 50 V, making the primary columns coarsen and coalesce to form eventually a single column under each box [image (b)]. After 4.5 min, when the voltage is further increased to 100 V, secondary columns at the intersection of the channels appear as shown in the image (c). After another 2 min, ramping up the applied voltage to 130 V causes smaller tertiary columns to appear in the channels between the boxes [image (e)]. The simulated images (i)–(v) very closely emulate the experimental results under the similar set of conditions. Image (i) shows the box-patterned top electrode with box dimensions of

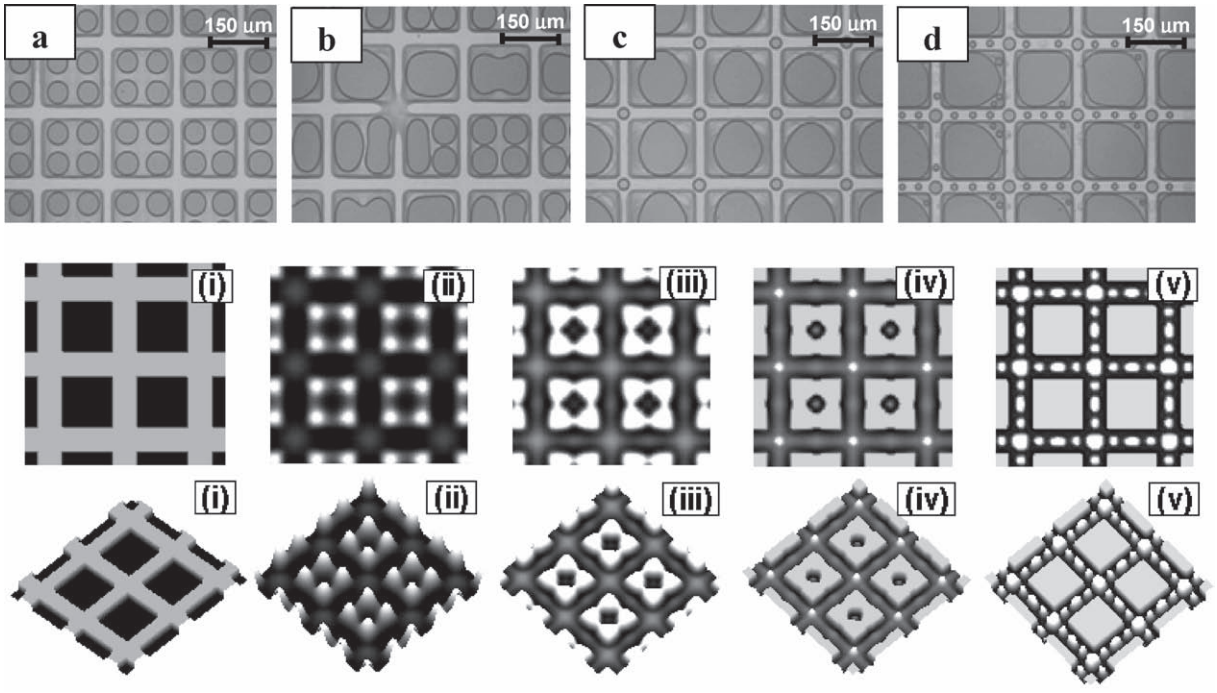

Figure 10. Optical micrographs (a)–(e) show patterning of a 7.7 μm film. Image (a) shows the formation of four primary columns per box of dimension 150 × 150 μm under the voltage bias of 30 V for 50 s (box dimension ~ 2λ). The height of the box-patterns on the top electrode is ~ 1 μm. After 30 s, the voltage is increased to 50 V. Image (b) shows the coalescence of these columns at 50 V after 2.5 min. The voltage is ramped up to 100 V after 4.5 min. Image (c) shows the appearance of smaller secondary columns at the corners between the boxes on applying a voltage bias of 100 V for 2 min. Thereafter, the voltage is increased to 130 V. Image (d) shows the formation of tertiary columns between the boxes on exposure to 130 V for 9 min. Images (i)–(v) show simulated patterns for a 7 μm film under a patterned electrode having boxes of dimension 2λ. The dimensionless distance of the boxes [darker region in image (i)] and grooves [lighter region in image (i)] on the patterned electrode from the film surface are 1.5 and 1.8, respectively. Image (ii) shows four primary columns per box under the ridges at 30 V after $T = 1.33 \times 10^2$. Image (iii) shows coalescence of structures under the boxes at 50 V and after $T = 1.68 \times 10^2$. Image (iv) shows appearance of secondary columns under the grooves at the corner of the box-patterns when the voltage is ramped up to 100 V after $T = 1.77 \times 10^2$. Image (v) shows appearance of tertiary columns at under the grooves and in between the box patterns when the voltage bias is ramped up to 130 V after $T = 2.1 \times 10^2$. In the simulated pictures, lighter shades of gray indicate the regions with higher film thickness.

2λ. In the beginning, 30 V electric field bias leads to the formation of a quartet of primary columns on each box-pattern [image (ii)]. Following this, when the voltage is ramped up to 50 V, the columns under the boxes start coalescing [image (iii)]. Thereafter, increasing the voltage to 100 V leads to the coalescence of the structures and secondary columns make their appearance [image (iv)]. Finally, when the electric field is further stepped up to 130 V, tertiary columns appear all along the channels; the spacing between them being determined by the spinodal wavelength corresponding to this set of conditions.

In Figure 11, we show that using the same top box-patterned electrode, ordering of patterns can further be altered by varying the initial voltage bias. At initial electric field bias of 50 V, nine primary columns arranged on a square lattice appear on each box as shown in the images (a) and (b). The voltage is increased to 90 V after 1 min, leading to secondary columns at the intersection of channels [image (c)] and progressive coalescence of the primary columns. After 3 min of exposure to 90 V electric field, the voltage is further ramped up to 130 V and smaller tertiary columns now appear in the channels [image (d)]. The simulated results for this system are portrayed in the images (i) – (iv), which again closely resembles the key features of evolution. Image (i) shows the box-patterned top electrode with box dimension 3.125λ when the film thickness is 7 μm and applied voltage is 50 V.

It is important to note here that the initial film thickness plays a key role in the higher order hierarchical structure formation. The experiments indicate that a thicker film is more conducive to fabricate higher order hierarchical structures at lower voltages because of the availability of more material after the formation of the primary/secondary structures. For thinner films, a stronger electric field in the beginning becomes necessary because the primary structures in this case deplete the film less and enough material is still left for the formation of higher order structures. The examples discussed here point to the fact that TeMo-EFL can be employed to fabricate complex multiscale micro/nano architectures that may be useful for fabrication in applications related to sensors, microfluidic devices, microelectronics, functional surfaces (e.g., superhydrophobic), solar cells and fuel cell electrodes.

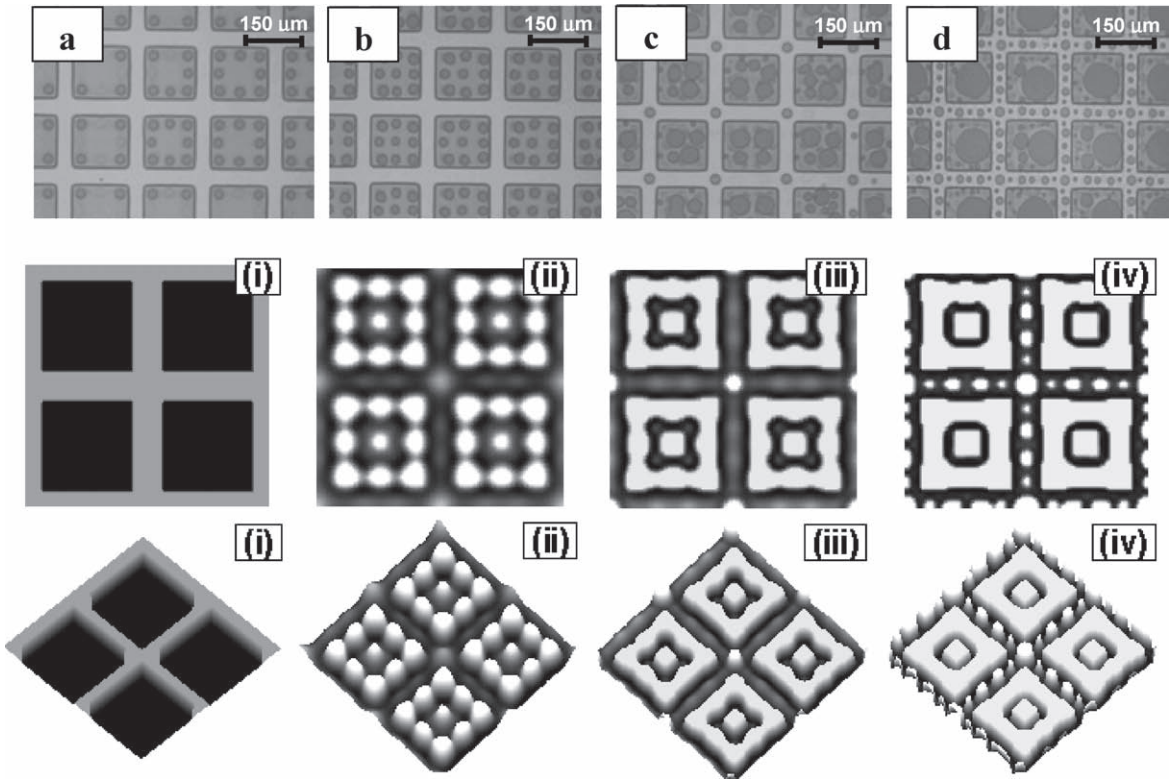

Figure 11. Optical micrographs (a)–(d) show patterning of a 7.8 μm film. Images (a) and (b) show the evolution of nine primary columns under each square box of dimension 150 × 150 μm when 50 V electric field bias is applied for 1 min (box dimension ~ 3λ). After this the voltage bias is increased to 90 V for 3 min and image (c) shows the appearance of smaller secondary columns at the corners of the boxes. Meanwhile, the columns under the boxes had started to coalesce. Thereafter, voltage bias is increased to 130 V for 3 min and image (d) shows the formation of further smaller tertiary columns in the channels between the boxes. Images (i)–(iv) show simulated patterns on a 7 μm film under a patterned electrode having boxes of dimension 3.125λ. The dimensionless distance of the boxes [darker region in image (i)] and grooves [lighter region in image (i)] on the patterned electrode from the film surface are 1.6 and 1.8, respectively. Image (ii) shows nine primary columns under the box patterns at 50 V and $T = 1.2 \times 10^2$. Image (iii) shows appearance of secondary columns at the corner of the box patterns when the voltage is ramped up to 90 V and at $T = 1.3 \times 10^2$. Image (iv) shows appearance of tertiary columns between the channels of the box patterns at 130 V and $T = 1.56 \times 10^2$. In the simulated pictures, lighter shades of gray indicate the regions with higher film thickness.

3. Conclusions

A new methodology is proposed for the fabrication of mesopatterns in cross-linkable PDMS films by guiding the self-organization using a programmable temporal variation of the electric-field. In particular, hierarchical structures of increasing complexity can be obtained even by the use of simply patterned electrodes and multiple structures can be fabricated with the same electrode by a temporal variation of the field. The integrity of the structures formed at different times and in the postcuring phase is preserved by an incomplete cross-linking of PDMS which imparts greater viscoelasticity and minimizes the structural distortion and ripening. Use of simulations in prediction of structures adds to a rational use of the proposed TeMo-EFL. The methodology is suitable not only for PDMS, but also for other photo- or heat cross-linkable materials. The key specific observations related to pattern formation are: I) It is the width, rather than the periodicity of electrode-patterns, that largely govern the structural morphology of the columns. For example, when the width of elevated stripes (or boxes) on the electrode is between λ and 2λ, a single row (or single) of column is observed; but ordered doublet or triplet lines of columns can be formed when the width is in the range of 2λ to 3λ and 3λ to 4λ, respectively, without losing the order. II) The patterns produced depend on the initial starting voltage and the duration of its application for a film and electrode combination. III) Multiscale structures with increasingly finer secondary, tertiary and quaternary structures are formed by imposing increments in the voltage. The structures thus fabricated can be far more complex than the electrode topography and can even be modulated by imposing different temporal variations of the field. This work thus extends the scope and promise of EFL.

4. Experimental Section: Preparation of the Film and Electrodes

The schematic diagram of the experimental setup is shown in the images (a) to (d) in the Figure 1. The parallel plate capacitor geometry in the experiments is composed of two plates, a contactor or electrode at the top, a substrate at the bottom and a polymer film coated on the substrate. The top electrode and the substrate are made of precleaned ITO coated glass (SPI supplies, USA; polished ITO, 8–12 Ω). The polymer film is the

commercially available Sylgard-184 (two part PDMS elastomer; Dow Chemicals, USA), which is composed of an oligomer and a cross-linking agent. The oligomer and the crosslinker (10% by weight) were dissolved in n-Hexane and then spin coated on the substrate. Films of thicknesses varying from 3 μm to 13 μm were prepared by varying the amount of the solvent in the solution and the spin speed (1100 rpm to 2500 rpm). After coating, the films were left in air for 4 h to relax excess stresses because of the spin coating. The films were partially cured at 105 °C for 10 min to 90 min to obtain films with different extent of viscoelasticity. Partial curing increases the viscosity and infuses some elasticity in the films, which resists the coalescence of the patterns during the patterning phase and in the postpatterning phase. However, precuring for a longer time converts the polymer film into an elastic solid, which was avoided. The precuring time was optimized using a flat top electrode and the experiments with patterned top electrodes were performed later by using the PDMS with optimized precuring time. Best results were obtained with 45–60 min of partial precuring at 105 °C.

The patterned contactors or electrodes (Figure 3) were fabricated by using a Maskless Photolithography setup (Intelligent Micropatterning, USA) and a positive photo-resist, Shipley 1818. The photo-resist was diluted using its thinner and then spin coated on the electrode. Various thicknesses (30 nm to 2.5 μm) of photo-resist coatings were fabricated by varying the spin speed from 3000 rpm to 5000 rpm. The maskless photolithography technique allowed us to control the variation of UV light intensity in the same optical frame thus allowing the fabrication of the outer rectangular spacer and the pattern inside in a single step. The outer rectangular spacer had a thickness of 2.5 μm and the electrode pattern within had a maximum thickness of 2.47 μm, thus creating the minimum air-gaps of 30 nm (Figure 3). Three types of patterned top electrodes were fabricated for experiments: i) alternate parallel ridges and valleys (Figure 3a), ii) elevated concentric circular rings (Figure 3b), and iii) elevated isolated boxes (Figure 3c). The coating thickness on the contactor was measured by contact profilometry. The patterned dielectric coating of the photoresist created the spatially varying electric field. In the beginning of the experiments, the patterned contactor and the substrate with coated partially cured polymer films were placed in a parallel plate capacitor arrangement and connected to a 0–200 V DC source through copper tapes. The deformations on the film surface with time were followed by an optical microscope (Leica DMLM) and the images were captured using a digital camera. The wavelengths of the patterns obtained were also verified by FFT of the optical micrographs. Once the desired patterns were obtained, the voltage bias was switched off and the film with its electrodes in place was immediately transferred to a furnace at a temperature of 110 °C for 24 h. This postcuring transformed the soft polymer to a solid film because of the presence of excess cross-linker. Thereafter, the top electrode was removed and patterned film was slowly cooled.

5. Theory and Simulations

Image (e) in Figure 1 schematically shows the deformation of a thin film under the influence of an external electric field. The polymeric film is considered to be a thin, isothermal, linear isotropic dielectric, incompressible and Newtonian liquid. The film ($0 \le z \le h$) is confined in air ($h \le z \le d$) and the voltage (ψ_b) is applied through bounding electrodes (substrate and the contactor). It is also assumed that the material properties of the films such as, viscosity (μ), dielectric constant (ε_p) and surface tension (γ) are constant.

5.1. Problem Formulation

The following thin film equation, derived from the long-wave Navier–Stokes equation and subjected to the boundary conditions: (a) no slip and impermeability at the film-substrate interface, and (b) shear stress balance at the film-air interface, governs the dynamics of a thin liquid film on a homogeneous surface, when exposed to an external electric field:[8–10,65,77]

$$3\mu\,(\partial h/\partial t) - \nabla\cdot\left(h^3\nabla P\right) = 0. \tag{1}$$

At the free interface, $z = h$ (x, y, t), the normal stress condition relates the total pressure to the curvature, the intermolecular conjoining pressure and the stresses because of the electrostatic field:[65,77]

$$P = p_0 - \gamma\nabla^2 h + \phi \tag{2}$$

Here p_0 is the ambient pressure. The potential (ϕ) for the film is defined as follows:[65,77]

$$\phi = -\frac{\varepsilon_0\varepsilon_p(\varepsilon_p-1)\psi^2}{2\left[\varepsilon_p d-(\varepsilon_p-1)h\right]^2} - \frac{A}{6\pi h^3} + \frac{B}{(d-h)^7}. \tag{3}$$

Here ε_0 is the permittivity in the free space and A is an effective Hamaker constant ($A = A_{ff}–A_{sf}$), where the subscripts s and f represent the lower electrode and the PDMS liquid, respectively. The lower electrode is considered to be completely wettable by the PDMS film in the absence of an electric field, implying $A_{ff} < A_{sf}$. To avoid the contact-line singularity and ensure non-penetration of liquid in the top electrode at contact, the polymer film is also subjected to a steep repulsion $[B/(d-h)^7]$ when the air gap thickness become very small ($d - h \sim l_0$). The parameter B is evaluated using the condition conjoining pressure $\phi = 0$ at $h = d - l_0$, where l_0 is a cutoff thickness. The short-range van der Waals repulsion at the bottom electrode has been incorporated to ensure a precursor layer of thickness $h > l_0$, which avoids the non-physical singularity associated with the film breakup.[8–10,65] However, this van der Waals repulsion force in Equation (3) has a negligible influence on pattern formation compared to the effect of the much stronger electrostatic term.

The gradient of potential, ∇P, in Equation (1) includes the force because of the local film thickness variations, $(\partial\phi/\partial h)\nabla h$, and also the force resulting from the imposed spatial heterogeneity of the electric field, which is imposed by a topographically patterned top-electrode. The first component of force, $-(\partial\phi/\partial h)\nabla h$ at a given location, engenders the spinodal instability of a spatially homogeneous field by causing a flow from the thinner to thicker regions of the film. The second force due to the heterogeneity of the electric field, at constant film

thickness, moves the fluid from the low to high regions of electric field, for example, from the regions where the electrode spacing is higher to where it is lower.[65,77] The linear stability analysis of the dimensional thin film equation [Equation (1)] provides simple qualitative scaling to assess the length scale of the instability. In this study, we often report this wavelength while discussing the experimental and theoretical results. The dominant wavelength λ obtained for a film of base state thickness h_0 from the linear theory is:[47,65]

$$\lambda = 2\pi \sqrt{\frac{2\gamma\left[\varepsilon_p d - (\varepsilon_p - 1)h_0\right]^3}{\varepsilon_0 \varepsilon_p (\varepsilon_p - 1)^2 \psi^2}}. \quad (4)$$

5.2. Numerical Methods

Equation (1) is made dimensionless for the sake of compactness employing the following dimensionless variables $H = h/h_0$, $\Phi = \left(\phi h_0^3/A\right)$, $X = Kx/h_0$, $Y = Ky/h_0$, $T = t/\left(3\mu h_0/\gamma K^4\right)$ where $K = \sqrt{A/\gamma h_0^2}$. The dimensionless form of the equation thus obtained has the following form:

$$\partial H/\partial T + \nabla.\left[H^3 \nabla\left(\nabla^2 H\right)\right] - \nabla.\left[H^3 \nabla \Phi\right] = 0. \quad (5)$$

Here H, Φ, X, Y, T are the nondimensional film thickness, conjoining pressure, X-coordinate, Y-coordinate, and time, respectively. Equation (5) is numerically solved using a central difference scheme in space (X and Y) combined with Everett interpolation method and periodic boundary conditions at the edges. The film is perturbed randomly in the beginning ($T = 0$) to initiate the instabilities and Gear's algorithm for stiff equations is employed for the time marching. The grid spacing is always kept uniform ($\Delta X = \Delta Y$) and convergence of results was verified by increasing the grid density.

The method of simulations is briefly presented here, but more details can be obtained elsewhere.[65] The method has been found successful in reproducing the morphological evolution in films subjected to a spatially varying field.[64,65,68,77] Further, it is known that the length scale and morphology of instability is independent of the liquid viscoelasticity, which however alters the dynamics.[71] The simulations reported here are thus an approximation, especially in the late phases of pattern formation governed by the rapidity of the processes of ripening and coalescence.

Acknowledgements

PSGP and IB have contributed equally to this work. AS acknowledges the support of the DST, New Delhi through an IRHPA grant and the World Class University Grant No. R32–2008-000–20082-0 of the Ministry of Education, Science and Technology of Korea. PSGP and IB thanks Rabibrata Mukherjee for insightful discussions and Srikant for helping with profilometric measurements.

Received: June 14, 2010
Revised: July 28, 2010
Published online: November 10, 2010

[1] E. Ruckenstein, R. K. Jain, *J. Chem. Soc., Faraday Trans. 2* **1974**, *70*, 132.
[2] P. G. De Gennes, *Rev. Mod.Phys.* **1985**, *57*, 827.
[3] G. Reiter, *Phys. Rev. Lett.* **1992**, *68*, 75.
[4] F. Brochard-Wyart, P. Martin, C. Redon, *Langmuir* **1993**, *9*, 3682.
[5] A. Sharma, *Langmuir* **1993**, *9*, 861.
[6] G. Reiter, *Langmuir* **1993**, *9*, 1344.
[7] A. Oron, S. H. Davis, S. G. Bankoff, *Rev. Mod. Phys.* **1997**, *69*, 931.
[8] A. Sharma, R. Khanna, *Phys. Rev. Lett.* **1998**, *81*, 3463.
[9] R. Konnur, K. Kargupta, A. Sharma, *Phys. Rev. Lett.* **2000**, *84*, 931.
[10] K. Kargupta, A. Sharma, *Phys. Rev. Lett.* **2001**, *86*, 4536.
[11] U. Thiele, M. Velarde, K. Neuffer, *Phys. Rev. Lett.* **2001**, *87*, 016104.
[12] L. Brusch, H. Kühne, , M. Bär, *Phys. Rev. E* **2002**, *66*, 011602.
[13] A. Sehgal, V. Ferreiro, J. F. Douglas, E. J. Amis, A. Karim, *Langmuir* **2002**, *18*, 7041.
[14] Z. Zhang, Z. Wang, R. Xing, Y. Han, *Surface Science* **2003**, *539*, 129.
[15] G. Narsimhan, *J. Coll. Int. Sci.* **2005**, *287*, 624.
[16] M. H. Yang, S. Y. Hou, Y. L. Chang, A. C.-M. Yang, *Phys. Rev. Lett.* **2006**, *96*, 066105.
[17] G. G. Baralia, C. Filiatre, B. Nysten, A. M. Jones, *Adv. Mat.* **2007**, *19*, 4453.
[18] D. Julthongpiput, W. H. Zhang, J. F. Douglas, A. Karim, J. M. Fasolka, *Soft Matter* **2007**, *3*, 613.
[19] H. Krishna, N. Shirato, C. Favazza, R. Kalyanaraman, *Phys.Chem. Chem. Phys.* **2009**, *11*, 8136.
[20] O. Wunnicke, P. Müller-Buschbaum, M. Wolkenhauer, C. Lorenz-Haas, R. Cubitt, V. Leiner, M. Stamm, *Langmuir* **2003**, *19*, 8511.
[21] O. K. Matar, V. Gkanis, S. Kumar, *J. Coll. Int. Sci.* **2005**, *286*, 319.
[22] X. Zhang, F. Xie, O. K. C. Tsui, *Polymer* **2005**, *46*, 8416.
[23] J. H. Wei, D. C. Coffey, D. Ginger, *J. Phys. Chem. B* **2006**, *110*, 24324.
[24] C. P. Martin, M. O. Blunt, E. Pauliac-Vaujour, A. Stannard, P. Moriarty, *Phys. Rev. Lett.* **2007**, *99*, 116103.
[25] R. Mukherjee, D. Bandyopadhyay, A. Sharma, *Soft Matter* **2008**, *4*, 2086.
[26] J. C. T. Kao, A. A. Golovin, S. H. Davis, *J. Coll. Int. Sci.* **2006**,*303*, 532.
[27] S. Saprykin, P. M. Trevelyan, R. J. Koopmans, S. Kalliadasis, *Phys. Rev. E* **2007**, *75*, 026306.
[28] R. V. Craster, O. K. Matar, *Rev. Mod. Phys.* **2009**, *81*, 1131.
[29] R. D. Lenz, S. Kumar, *J. Fluid Mech.* **2007**, *571*, 33.
[30] G. Reiter, M. Hamieh, P. Damman, S. Sclavons, S. Gabriele, T. Vilmin, E. Raphaël, *Nat. Mater.* **2005**, *4*, 754.
[31] R. L. Jones, T. J. Hu, C. L Soles, E. K. Lin, R. M. Reano, P. W. Stella, D. M. Casa, *Nano Lett.* **2006**, *6*, 1723.
[32] A. A. Golovin, M. S. Levine, T. V. Savina, S. H. Davis, *Phys. Rev. B* **2004**, *70*, 235342.
[33] A. Ghatak, M. K. Chaudhury, V. Shenoy, A. Sharma, *Phys. Rev. Lett.* **2000**, *85*, 4329.
[34] W. Monch, S. Herminghaus, *Europhys. Lett.* **2001**, *53*, 525.
[35] V. Shenoy, A. Sharma, *Phys. Rev. Lett.* **2001**, *86*, 119.
[36] C. Q. Ru, *J. Appl. Phys.* **2001**, *90*, 6098.
[37] V. Shenoy, A. Sharma, *J. Mech. Phys. Solids* **2002**, *50*, 1155.
[38] A. Ghatak, M. K. Chaudhury, *Langmuir* **2003**, *19*, 2621.
[39] J. Sarkar, V. Shenoy, A. Sharma, *Phys. Rev. Lett.* **2004**, *93*, 018 302.
[40] S.-Q. Huang, Q.-Ya. Li, X.-Q. Feng, S.-W. Yu, *Mech. Mater.* **2006**, *38*, 88.
[41] M. Gonuguntla, A. Sharma, J. Sarkar, S. A. Subramanian, M. Ghosh, V. Shenoy, *Phys. Rev. Lett.* **2006**, *97*, 018303.
[42] J. Sarkar, A. Sharma, *Langmuir* **2010**, *26*, 8464.
[43] S. Y. Chou , L. Zhuang, *J. Vac. Sci. Technol. B* **1999**, *17*, 3197.
[44] S. Y. Chou, L. Zhuang , L. Guo, *Appl. Phys. Lett.* **1999**, *75*, 1004.
[45] P. Deshpande, X. Sun , S. Y. Chou, *Appl. Phys. Lett.* **2001**, *79*, 1688.
[46] S. Herminghaus, *Phys. Rev. Lett.* **1999**, *83*, 2359.

[47] E. Schaffer, T. Thurn-Albrecht, T.P Russel, U. Steiner, *Nature* **2000**, *403*, 874.
[48] E. Schaffer, T. Thurn-Albrechet, T. P. Russell, U. Steiner, *Europhys. Lett.* **2000**, *53*, 518.
[49] Z. Lin, T. Kerle, S. M. Baker, D. A. Hoagland, E. Schaffer, U. Steiner, T. P. Russell, *J. Chem. Phys.* **2001**, *114*, 2377.
[50] Z. Lin, T. Kerle, T. P. Russell, E. Schaffer, U. Steiner, *Macromolecules* **2002**, *35*, 3971.
[51] Z. Q. Lin, T. Kerle, T. P. Russell, E. Schaffer, U. Steiner, *Macromolecules* **2002**, *35*, 6255.
[52] L. F. Pease III, W. B. Russel, *J. Non-Newtonian Fluid Mech.* **2002**, *102*, 233.
[53] M. D. Morariu, N. E. Voicu, E. Schäffer, Z. Lin, T. P. Russell, U. Steiner, *Nat. Mater.* **2003**, *2*, 48.
[54] S. Harkema, E. Schäffer, M. D. Morariu, U. Steiner, *Langmuir* **2003**, *19*, 9714.
[55] T. Xu, C. J. Hawker, T. P. Russell, *Macromolecules* **2003**, *36*, 6178.
[56] Pease, L. F., III; Russel, W. B., *Langmuir* **2004**, *20*, 795.
[57] H. Xiang, Y. Lin, T. P. Russell, *Macromolecules* **2004**, *37*, 5358.
[58] V. Shankar, A. Sharma, *J. Coll. Int. Sci.* **2004**, *274*, 294.
[59] R. V. Craster, O. K. Matar, *Phys. Fluids.* **2005**, *17*, 032104.
[60] N. Wu, W. B. Russel WB*Appl. Phys. Lett.* **2005**, *86*, 241912.
[61] X. F. Wu, Y. A. Dzenis YA, *J Phys. D Appl. Phys.* **2005**, *38*, 2848.
[62] K. A. Leach, Z. Lin, T. P. Russell, *Macromolecules* **2005**, *38*, 4868.
[63] K. A. Leach, S. Gupta, M. D. Dickey, C. G. Wilson, T. P. Russell, *Chaos* **2005**, *15*, 047506.
[64] S. Harkema, U. Steiner, *Adv. Funct. Mater.* **2005**, *15*, 2016.
[65] R. Verma, A. Sharma, K. Kargupta, J. Bhaumik, *Langmuir* **2005**, *21*, 3710.
[66] N. Wu, L. F. Pease, III, W. B. Russel, *Langmuir* **2005**, *21*, 12290.
[67] N. Wu, L. F. Pease, III, W. B. Russel, *Adv. Funct. Mater.* **2006**, *16*, 1992.
[68] N. E. Voicu, S. Harkema, U. Steiner, *Adv. Funct. Mater.* **2006**, *16*, 926.
[69] N. Arun, A. Sharma, V. Shenoy , K. S. Narayan, *Adv. Mater.* **2006**, *18*, 660.
[70] M. D. Dickey, E. Collister, A. Raines, P. Tsiartas,T. Holcombe, S. V. Sreenivasan, R. T. Bonnecaze, C. G. Willson, *Chem. Mater.* **2006**, *18*, 2043.
[71] G. Tomar, V. Shankar, A. Sharma, G. Biswas, *J. Non-Newtonian Fluid Mech.* **2007**, *43*, 120.
[72] H. K. Yeoh, Q. Xu, O. Basaran, *Phys. of Fluids* **2007**, *19*, 114111.
[73] J. Sarkar, A. Sharma, V. Shenoy, *Phys. Rev. E* **2008**, *77*, 031604.
[74] K. John, P. Hänggi, U. Thiele, *Soft Matter* **2008**, *4*, 1183.
[75] J. Bae, E. Glogowski, S. Gupta S, W. Chen, T. Emrick, T. P. Russell, *Macromolecules* **2008**, *41*, 2722.
[76] M. D. Dickey, A. Raines, E. Collister, C. G. Willson, *J. Mat. Sci.* **2008**, *43*, 117.
[77] X. N. Xie, H. J. Chung, D. Bandyopadhyay, A. Sharma, C. H. Sow, A. A. Bettiol, A. T. S. Wee. *J. App. Phys.* **2008**, *103*, 024307.
[78] J. Heier, J. Groenewold, U. Steiner, *Soft Matter* **2009**, *5*, 3997.
[79] S. A. Roberts, S. Kumar, *J. Fluid Mech.* **2009**, *631*, 255.
[80] N. Wu, W. B. Russel, *Nano Today* **2009**, *4*, 180.
[81] N. Arun, A. Sharma, P. S. G. Pattader, I. Banerjee, H. M. Dixit, K. S. Narayan, *Phys. Rev. Lett.* **2009**, *102*, 254502.
[82] S. Manigandan, S. Majumder, A. Suresh, S. Ganguly, K. Kargupta , D. Banerjee, *Sens. Actuators B* **2010**, *144*, 170.